JOURNAL OF COMPUTATIONAL PHYSICS **146,** 322–345 (1998)
ARTICLE NO. CP986061

An Implicit Multigrid Method for the Simulation of Chemically Reacting Flows

P. Gerlinger, P. Stoll, and D. Brüggemann

Universität Stuttgart, Pfaffenwaldring 31, 70550 Stuttgart, Germany

Received December 31, 1997; revised July 20, 1998

The application of multigrid methods is complicated if the set of governing equations contains strongly nonlinear source terms. This is the case for finite-rate chemistry as well as for turbulence conservation equations. In most cases strong nonlinearities within the chemical production rates prevent convergence of standard multigrid methods. This paper investigates different approaches to treating chemical and turbulent production terms on coarse grids in order to enable convergence. Independent of combustion, supersonic flows require special care during restriction and prolongation if strong shock waves occur. A full coarsening four-level nested multigrid method is used for all conservation equations including those of turbulence and species transport. Strong convergence accelerations are achieved by a local source term-dependent damping of the restricted residual error. Several test cases with and without combustion demonstrate the efficiency and accuracy of the proposed multigrid algorithm.

Key Words: multigrid; combustion; supersonic flows; finite-rate chemistry.

1. INTRODUCTION

The simulation of chemically reacting flows using finite-rate chemistry still requires tremendous computer time, making convergence accelerations extremely necessary. For nonreactive flows multigrid techniques belong to the most efficient methods to reach a steady state solution. They have first been employed to elliptic subsonic flows, where excellent results may be achieved [1–3]. Jameson *et al.* [4, 5] developed an implicit multigrid method for transonic flows. Modifications also allow the calculation of supersonic and hypersonic problems [6–15]. Due to their hyperbolic character, such cases require characteristic restriction and prolongation operators [11] or a damping of the transferred residual errors at shock waves [12–15]. Even if the achieved convergence accelerations for supersonic flows are smaller than those for subsonic cases, a strong reduction in computer time is demonstrated by all authors cited above.

0021-9991/98 $25.00

Very little work has been done on application of multigrid methods if the set of governing equations includes strongly nonlinear source terms. Difficulties often arise due to widely disparate time and length scales which in the case of finite-rate chemistry may differ many orders in magnitude. The resulting numerical stiffness is usually treated with implicit or at least point-implicit numerical methods for time integration. Therefore the multigrid technique has to be adapted for implicit schemes also. Convergence acceleration of multigrid methods is based on the fact that low frequencies of the error are damped more efficiently on coarser grid levels. This is in contrast to the local behavior of turbulent or chemical production terms. If the source vector contains strongly nonlinear parts, coarse grid values strongly differ from corresponding fine grid values and therefore may no longer represent the problem on the finest grid. A second difficulty is that even small coarse grid corrections interpolated back to the finest grid may lead to strong changes within the source vector which can prevent convergence. Therefore special techniques are necessary to treat the nonlinear source terms as well as the corresponding source Jacobians on coarse grids. The problems arising from turbulent source terms are less severe than those due to chemistry, as the coupling between turbulence and fluid variables is quite weak. Even if low-Reynolds-number turbulence models are employed, multigrid methods may achieve considerable speedups. Liu and Zheng [16] use a point-implicit method, freezing turbulent production terms on coarse grids. In Refs. [14, 15], a coarse grid treatment for the turbulent source vector is presented that speeds up convergence to a steady state drastically even in cases of massively separated flows, shock wave/boundary layer interactions, and extreme cell aspect ratios.

Up to now, only a few papers have been published on the use of multigrid techniques for combustion calculations. Most of these papers achieved no or only small convergence accelerations. Slomski *et al.* [17] and Radespiel *et al.* [18] calculated reacting or dissociating air with small reaction schemes using standard multigrid procedures. Liao *et al.* [19–21] employed the multigrid technique for the momentum equations only without proving convergence accelerations. Considerable speedups are obtained by Sheffer *et al.* [22] for detonation waves using a two-level multigrid method. Most notably, Edwards [23] employed multigrid techniques for hypersonic chemically reacting flows and hydrogen combustion [24]. A global damping of the transferred residual error is used in Ref. [24] to enable convergence. This paper investigates several approaches on coarse grids to approximate chemical source terms and source Jacobians. The solution favored by the authors is a local damping of the restricted residual error in regions of high chemical activity. To our knowledge this is the first paper where a four-level multigrid method is successfully employed for diffusion-dominated flames and low-Reynolds-number turbulence closure.

2. GOVERNING EQUATIONS

The investigation of high-speed turbulent combustion requires the solution of the expanded Navier–Stokes equations which are given in two-dimensional form by

$$\frac{\partial \mathbf{Q}}{\partial t} + \frac{\partial (\mathbf{F} - \mathbf{F}_v)}{\partial x} + \frac{\partial (\mathbf{G} - \mathbf{G}_v)}{\partial y} = \mathbf{S}, \tag{1}$$

where the conservative variable vector is

$$\mathbf{Q} = [\rho, \rho u, \rho v, \rho E, \rho q, \rho \omega, \rho Y_i]^T, \qquad i = 1, 2, \ldots, N_s - 1. \tag{2}$$

F and **G** are inviscid, $\mathbf{F}_v$ and $\mathbf{G}_v$ are viscous fluxes in x- and y-directions, respectively. The source vector **S** results from turbulence and chemistry. The variables in Eq. (2) are the density ρ, the velocity components u and v, the total specific energy E, the turbulence variables $q = \sqrt{k}$ (k is the turbulent kinetic energy) and $\omega = \epsilon/k$ (ϵ is the dissipation rate of k), and the species mass fractions Y_i. N_s is the number of different species. The simulation of hydrogen combustion involves a 9-species (N_2, O_2, H_2, H_2O, OH, O, H, NO_2, and H_2O_2), 20-step reaction scheme developed by Jachimowski [25] excluding the nitrogen reactions. Fourth-order polynomials of temperature are employed for molecular viscosity, thermal conductivity, and diffusivity calculation of pure species. Mixture values of molecular viscosity and thermal conductivity are determined using Wilke's law [26], and diffusivity of one species in relation to the remaining gas is calculated according to Mason and Saxena [27]. Diffusion velocities and the associated heat flux terms are modeled using Fick's law. Turbulent contributions to thermal conductivity and diffusivity are obtained using constant turbulent Prandtl and Schmidt numbers. For turbulence closure a two-equation low-Reynolds-number q-ω model is employed [28–30].

A critical point for the multigrid method is the source vector appearing in Eq. (1) which is given by

$$\mathbf{S} = [0, 0, 0, 0, S_q, S_\omega, S_i]^T, \qquad i = 1, 2, \ldots, N_s - 1. \tag{3}$$

The turbulent source terms S_q and S_ω are calculated by [28]

$$S_q = C_{q1}\left(C_\mu D_q \frac{\mathcal{S}}{\omega^2} - \frac{2}{3}\frac{D}{\omega} - 1\right)\rho\omega q \tag{4}$$

$$S_\omega = \left[C_{\omega1}\left(C_\mu \frac{\mathcal{S}}{\omega^2} - C_{\omega3}\frac{D}{\omega}\right) - C_{\omega2}\right]\rho\omega^2 \tag{5}$$

and are also representative for other two equation turbulence closures. D is the divergence of the velocity field; $\mathcal{S}$ is the strain invariant; and C_{q1}, C_μ, $C_{\omega2}$, and $C_{\omega3}$ are modeling constants [29]. Two types of terms cause problems in multigrid methods: Terms formed by squares of velocity derivatives as the strain invariant,

$$\mathcal{S} = \left[2\frac{\partial u}{\partial x} - \frac{2}{3}\left(\frac{\partial u}{\partial x} + \frac{\partial v}{\partial y}\right)\right]\frac{\partial u}{\partial x} + \left(\frac{\partial u}{\partial y} + \frac{\partial v}{\partial x}\right)^2 + \left[2\frac{\partial v}{\partial y} - \frac{2}{3}\left(\frac{\partial u}{\partial x} + \frac{\partial v}{\partial y}\right)\right]\frac{\partial v}{\partial y}, \tag{6}$$

and exponential damping functions which depend on a turbulent Reynolds number R_q,

$$D_q = 1 - \exp(-0.022R_q), \qquad C_{\omega1} = 0.5D_q + 0.055. \tag{7}$$

Damping functions are necessary in many low-Reynolds-number turbulence models for an accurate simulation of the logarithmic near wall behavior. Like chemistry, turbulent production and dissipation are local phenomena. Nevertheless, there is a strong difference between turbulent and chemical source terms. While chemical production terms only depend on local values of the variable vector, turbulent production terms also depend on flow variable derivatives which in discretized form require values from neighboring cells. Therefore, the resulting value of these terms (e.g., $\mathcal{S}$) is strongly grid size (grid level) dependent. Like chemical source terms, turbulent damping functions (e.g., D_q) cause problems in the

multigrid method due to their local nonlinear behavior. The turbulent Reynolds number depends linearly on the distance of a cell center to the nearest wall. Especially close to solid walls, differences in wall distances at different grid levels cause strong changes within these exponential damping functions. For cases with flow separation a coarse grid recalculation of these terms may prevent convergence [14].

3. NUMERICAL METHOD

The unsteady form of governing equations is integrated in time using an implicit finite-volume LU algorithm [4, 31]. Jameson and Yoon [32] have demonstrated the ability of this driving scheme to rapidly damp out high-frequency error modes. This is a basic and necessary feature for an algorithm to be used as a smoother for multigrid methods. In addition to the inviscid Jacobians, simplified viscous Jacobians are included in the implicit part based on the thin-layer Navier–Stokes equations. In Eq. (8) this is shown for the η-direction only. The discretized implicit LU scheme is given by [31]

$$\begin{aligned}&\big[\mathbf{I} + \Delta t\big(\tilde{\mathbf{A}}^{+}_{i,j} - \tilde{\mathbf{A}}^{-}_{i,j} + \tilde{\mathbf{B}}^{+}_{i,j} - \tilde{\mathbf{B}}^{-}_{i,j} + 2\tilde{\mathbf{T}}_{i,j} - \tilde{\mathbf{H}}_{i,j}\big) - \Delta t\big(\tilde{\mathbf{A}}^{+}_{i-1,j} + \tilde{\mathbf{B}}^{+}_{i,j-1} + \tilde{\mathbf{T}}_{i,j-1}\big)\\ &\quad - \Delta t\big(\tilde{\mathbf{A}}^{-}_{i+1,j} + \tilde{\mathbf{B}}^{-}_{i,j+1} + \tilde{\mathbf{T}}_{i,j+1}\big)\big]\Delta\mathbf{Q}_{i,j} = \Delta t\mathbf{R}_{i,j}. \end{aligned} \tag{8}$$

To ensure diagonal dominance the upwind differenced inviscid Jacobians on the cell interfaces $\tilde{\mathbf{A}}$ and $\tilde{\mathbf{B}}$ are split in $+$ and $-$ matrices containing only positive or negative eigenvalues [4, 31]. $\mathbf{T}$ are centrally differenced Jacobians of the viscous fluxes, and $\mathbf{H} = \partial\mathbf{S}/\partial\mathbf{Q}$ is the source Jacobian due to chemistry and turbulence. The turbulence equations are solved in a loosely coupled form with the fluid motion. Finally $\mathbf{R}$ is the discretized residual. If the diagonal, lower, and upper Jacobians of Eq. (8) are combined to form D, L, and U, this equation can be expressed by

$$(D + L + U)\Delta\mathbf{Q}^{n+1} = -\Delta t\mathbf{R}. \tag{9}$$

Approximately factored, Eq. (9) is solved in two steps [31]:

Lower sweep:

$$(D + L)\Delta\bar{\mathbf{Q}} = -\Delta t\mathbf{R}. \tag{10}$$

Upper sweep:

$$(D + U)\Delta\mathbf{Q}^{n+1} = D\Delta\bar{\mathbf{Q}}. \tag{11}$$

The solution is updated by $\mathbf{Q}^{n+1} = \mathbf{Q}^{n} + \Delta\mathbf{Q}^{n+1}$. The source and viscous Jacobians add to the diagonal D, forming a matrix which has to be inverted directly at every grid point. An approximation for the chemistry source Jacobian has been proposed by Eberhardt and Imlay [33], resulting in a diagonal matrix only. However, the computational, more expensive use of a full chemical source Jacobian is preferred in the present paper. Local time stepping is used to enhance convergence to a steady state.

As the right-hand side (RHS) is discretized with central differences, a second- and fourth-order matrix dissipation is added to reduce oscillations near shock waves and to enable convergence to machine accuracy [34, 35].

4. THE MULTIGRID METHOD

A full coarsening multigrid method based on the full approximation storage (FAS) scheme of Brandt [2, 36] is used. The implicit version for approximately factored schemes was first presented by Jameson and Yoon [4]. Coarse grids are formed by eliminating every other grid line of the previous finer mesh.

If multigrid methods are used for chemically reacting flows, problems arise from the strongly nonlinear source vector. Chemistry is a local phenomenon, and the basic features of multigrid such as damping out low-frequency errors do not work. However, convergence accelerations are possible by using larger time steps. A necessary condition is the stability of the chemical time integration scheme and a time step limit, which allows such a procedure. The time step limit due to chemistry is supposed to be larger than that of convective and viscous contributions. In this case, convergence accelerations may be possible even in regions of disappearing convective fluxes. Because the time step due to convection and diffusion increases at least linearly with increasing grid level (for full coarsening), a significant advantage may be expected. So as to allow larger chemical time steps, the full analytically formed source Jacobian is used and chemistry is treated fully coupled with the fluid motion.

A V-cycle multigrid method is chosen for all simulations. The calculation is initialized by a nested iteration approach. The advantage of nested iterations is the provision of good initial distributions at low cost, leading to better convergence rates at the beginning of the calculation. For the simulation of chemically reactive flows a good initial guess still may be more important than in nonreactive cases. A steady state distribution of flow variables often causes fewer problems for multigrid time integration than transient states.

One iteration of the driving numerical scheme is expressed by rewriting Eqs. (10) and (11) to

$$\mathcal{F}^k \Delta \mathbf{Q}^k = \mathbf{R}(\mathbf{Q}^k), \tag{12}$$

where $\mathcal{F}^k = \mathcal{F}(\mathbf{Q}^k)$ is the implicit LU operator, $\mathbf{R}$ is the residual, and k indicates the grid level. Within one FAS V-cycle, the new iterate on the finest grid is calculated by the following steps:

Step 1: One relaxation sweep is carried out on the finest grid ($k = 1$) and the solution is updated.

Step 2: Initialization on the next coarser grid. The solution and the recalculated residuals are passed to the next coarser grid by

$$\mathbf{Q}_0^{k+1} = I_{k \mapsto k+1} \mathbf{Q}^k, \qquad \mathbf{R}_c^{k+1} = \bar{I}_{k \mapsto k+1} \mathbf{R}(\mathbf{Q}^k), \tag{13}$$

where the subscripts 0 and c represent the initialized coarse grid solution and the collected residuals, respectively.

Step 3: A coarse grid forcing function has to be calculated [4]. For $k = 1$ the forcing function is given by

$$\mathbf{P}^{k+1} = \mathbf{R}_c^{k+1} - \mathbf{R}\left(\mathbf{Q}_0^{k+1}\right), \tag{14}$$

while for $k > 1$,

$$\mathbf{P}^{k+1} = \bar{I}_{k \mapsto k+1} \mathbf{V}(\mathbf{Q}^k) - \mathbf{R}\left(\mathbf{Q}_0^{k+1}\right) \tag{15}$$

is used. The residual error at level $k+1$ is the sum of the forcing function and the calculated residual

$$\mathbf{V}^{k+1} = \mathbf{R}(\mathbf{Q}^{k+1}) + \mathbf{P}^{k+1}, \tag{16}$$

and the coarse grid solution is calculated similar to the procedure on the finest grid by

$$\mathcal{F}^{k+1}\Delta\mathbf{Q}^{k+1} = \mathbf{V}^{k+1}. \tag{17}$$

One iteration is performed at every grid level.

Step 4: If the coarsest grid is reached, the obtained coarse grid corrections are interpolated on the fine level and added to the old solution by

$$\mathbf{Q}^{k}_{\text{new}} = \mathbf{Q}^{k} + p_{k+1\mapsto k}\left(\mathbf{Q}^{k+1}_{\text{new}} - \mathbf{Q}^{0}_{k+1}\right). \tag{18}$$

No additional relaxation sweeps are performed on coarse grids after each prolongation step.

4.1. *Restriction and Prolongation*

The simulation of supersonic and hypersonic flows requires modifications during restriction and prolongation in comparison to standard (sub- or transonic) multigrid algorithms. This is due to the hyperbolic character of the governing equations. A pressure-based damping [12–15] of the restricted defect error is used in the present paper to avoid an unphysical upwind influence at shock waves which otherwise would prevent convergence. This method is numerically stable and computationally cheap, and allows one to treat even complicated flow structures. Koren and Hemker [12] have shown for inviscid hypersonic flows that a local damping of the restricted defect error improves robustness of the nonlinear multigrid method. Leclercq and Stoufflet [11] employed characteristic restriction and prolongation operators to solve the Euler equations. Especially for multicomponent flows, this mathematically correct treatment is computationally expensive, requiring matrix vector multiplications.

The following transfer operators are used for the applied full coarsening cell-centered finite-volume method.

- $I_{k\mapsto k+1}$ for restriction of the flow variables [4],

$$I_{k\mapsto k+1}\mathbf{Q}^{k} = \frac{1}{\Omega^{k+1}}\sum_{l=1}^{4}\Omega^{k}_{l}\mathbf{Q}^{k}_{l}, \tag{19}$$

where Ω^{k} is the corresponding cell area at grid level k. Four fine grid volumes are always collected forming one coarse grid volume.

- $\bar{I}_{k\mapsto k+1}$ for restriction of residuals and residual errors [13, 14],

$$\bar{I}_{k\mapsto k+1}\mathbf{R}^{k} = \sum_{l=1}^{4}\mathbf{R}^{k}_{l}\max\left(0, 1-\kappa^{k}_{l}\right), \qquad \bar{I}_{k\mapsto k+1}\mathbf{V}^{k} = \sum_{l=1}^{4}\mathbf{V}^{k}_{l}\max\left(0, 1-\kappa^{k}_{l}\right). \tag{20}$$

Instead of four fine grid residuals simply being added, the transfer is damped by parameter κ^{k}_{l}. This treatment is only necessary near shock waves which are located by the same sensor

as employed for adding artificial viscosity. Especially for multigrid applications we found it advantageous to use a blend between a standard pressure-based sensor [37] and a sensor with TVD properties [34],

$$\nu_{i,j}^{\xi} = \frac{|p_{i+1,j} - 2p_{i,j} + p_{i-1,j}|}{(1-\chi)(|p_{i+1,j} - p_{i,j}| + |p_{i,j} - p_{i-1,j}|) + \chi(p_{i+1,j} + 2p_{i,j} + p_{i-1,j})}, \quad (21)$$

which is given here for the ξ-direction. Values between 0.5 and 0.8 are used for χ in all of the following simulations. The damping parameter κ^k is formed by the maximum of some neighboring values of ν,

$$\kappa^k = C^k \max\left(\nu_{i,j}^{\xi}, \nu_{i-1,j}^{\xi}, \nu_{i+1,j}^{\xi}, \nu_{i,j}^{\eta}, \nu_{i,j-1}^{\eta}, \nu_{i,j+1}^{\eta}\right), \quad (22)$$

and constants C^k are used to adapt the damping factors to the decreasing smoothness of the pressure distribution on successively coarser grids.

- $p_{k+1\mapsto k}$ is a prolongation operator used to transfer corrections from coarse to fine grids. While in subsonic or smooth supersonic regions of the flowfield a second-order central prolongation operator is used (bilinear interpolation), a simple first-order upwind prolongation is employed near shock waves [38]. Again, the pressure-based sensor of Eq. (22) works as a switch between both kinds of prolongation operators.

In addition to the described damping of the transferred residual error, for implicit numerical schemes it is advantageous to reduce the coarse grid time step near shock waves. Instead of the standard time step Δt_s which is formed by convective and diffusive contributions, the following time step is employed:

$$\Delta t^k = \Delta t_s^k \max[\epsilon, (1-\kappa^k)^n] \qquad \text{for } k > 1. \quad (23)$$

The exponent n is necessary to adjust the coarse grid time step damping to different shock strengths, and ϵ is a limitation that usually is chosen to be 0.01.

4.2. *Treatment of Source Terms*

The greatest problem for multigrid solutions of turbulent reactive flows is the connection between fine grid source terms and their representation on coarse grids. In contrast to finite-rate chemistry, the coupling between turbulent source terms and fluid flow variables is quite weak, making the use of multigrid methods for the turbulence equations much more favorable. A simple freezing of nonlinear parts already enables convergence even in complicated cases with strong turbulence production and up to five grid levels [14, 15, 38]. For the q-ω model used, the strain invariant $\mathcal{S}$ and the damping function D_q are calculated on the finest grid only and passed to coarser grids by

$$\mathcal{S}^{k+1} = I_{k\mapsto k+1}\mathcal{S}^k, \qquad D_q^{k+1} = I_{k\mapsto k+1}D_q^k, \quad (24)$$

where they are kept constant. Because only these nonlinear contributions to the source term are kept constant, turbulent source term and source Jacobian are still able to react and to follow changes within the turbulent variables. This method is numerically very stable and works well even for massively separated flows.

The sensitivity of the chemical source terms

$$S_i = M_i \sum_{r=1}^{N_r} \left[(\nu''_{i,r} - \nu'_{i,r}) \left(k_{f_r} \prod_{l=1}^{N_k} c_l^{\nu'_{l,r}} - k_{b_r} \prod_{l=1}^{N_k} c_l^{\nu''_{l,r}} \right) \right], \qquad i = 1, 2, \ldots, N_s - 1 \quad (25)$$

to changes within the flow variables makes the treatment of finite-rate chemistry with multilevel multigrid much more difficult. The coupling is given by the species concentrations c_i and the exponential dependence of forward k_f and backward reaction rate k_b on temperature. An Arrhenius form is adopted for forward reaction rates while equilibrium constants are used to obtain backward reaction rates.

A linear transfer operator $I_{k \mapsto k+1}$ is used to restrict the flow variables to the next coarser grid in a conservative manner. Thus recalculation of strongly nonlinear source terms may cause strong differences within these terms at both grid levels (if gradients exist within the flow variables on the finer grid). If these differences become too strong, the relation between the grid levels gets lost, causing divergence of the multigrid algorithm. In the first three out of four investigated approaches, coarse grid source terms and Jacobians are approximated using additional information from the finest grid. This is done to separate coarse grid local production terms and Jacobians (which are fully or partially determined from the finest grid) from coarse grid variables.

- *Approach 1*: The chemical source terms and Jacobians are calculated on the finest grid only and are kept constant on coarser grids. While the coarse grid source terms are obtained by simply adding four fine grid values, the corresponding Jacobians are cell area weighted using $I_{k \mapsto k+1}$.
- *Approach 2*: The chemical source terms are treated in the same way as in approach 1. However, the transfer of chemical source Jacobian entries from fine to coarse grids is weighted using parameters that evaluate the chemical importance of the corresponding volume. The entries of the source Jacobian $\mathbf{H}$ are given by $H_{i,j}$ with $i, j = 1, 2, \ldots, N_s + 5$. All entries within the first six rows $i = 1, \ldots, 6$ of the source Jacobian are zero due to the absence of source terms (neglecting contributions from turbulence which are treated separately). While the columns $j = 1, \ldots, 6$ for $i = 7, \ldots, N_s + 5$ are determined using transfer operator $I_{k \mapsto k+1}$ the submatrix $i, j = 7, \ldots, N_s + 5$ is formed in a special way. First, the changes in gas composition

$$\Delta \tilde{\mathbf{Q}} = \left[0, 0, 0, 0, 0, 0, \Delta \tilde{Q}_1, \Delta \tilde{Q}_2, \ldots, \Delta \tilde{Q}_{N_s - 1} \right]^T \quad (26)$$

due to pure chemistry are calculated for every volume using local chemical production terms. Such a treatment additionally requires one to solve a set of $N_s - 1$ equations for every volume. The same time step Δt^k is used for the four fine grid volumes, forming one coarse grid volume. The fine grid changes $\Delta \tilde{Q}_i$ thereby achieved are now used for weighting the coarse grid Jacobians. The purpose of this procedure is to achieve coarse grid changes due to pure chemistry which approximate the cell area weighted changes of the four corresponding fine grid volumes. If geometric weighting factors for corresponding fine and coarse grid volumes are denoted by

$$v_l = \frac{\Omega_l^k}{\Omega^{k+1}}, \qquad l = 1, \ldots, 4, \quad (27)$$

coarse grid Jacobian entries are calculated by the expression

$$H^{k+1}_{i+6,\,j+6}\Omega^{k+1} = \frac{\sum_{l=1}^{4}\left(H^{k}_{i+6,\,j+6}\Omega^{k}\left|\Delta\tilde{Q}^{k+1}_{j}\right|\right)_{l}}{\sum_{l=1}^{4}\left(\left|\Delta\tilde{Q}^{k+1}_{j}\right|v\right)_{l}+\epsilon}, \qquad i,\,j=1,2,\ldots,N_s-1. \quad (28)$$

Absolute values of changes in species concentrations are used and ϵ is a small value to avoid a zero denominator. Every column of the coarse grid sub-Jacobian $i,\,j=7,\ldots,N_s+5$ is formed by weighting four corresponding fine grid columns with the same value. If four fine grid changes have the same sign, and if coarse and fine grid time steps are chosen identically, this Jacobian achieves a change on coarse grid which is identical to the four cell area weighted fine grid changes.

- *Approach 3*: The rates of forward and backward reaction are calculated on the finest grid only, transferred to coarser grids, and kept constant. Additionally, a transfer of temperature derivatives for the reaction rates is necessary to calculate coarse grid Jacobians. This approach was chosen because the most nonlinear dependence of the source term is due to temperature within the Arrhenius form. This approach still allows the coarse grid chemical production terms to vary due to changes in species densities.
- *Approach 4*: A new sensor is calculated to locate regions with high chemical intensity

$$\gamma = \left(\frac{1}{N_s-1}\sum_{i=1}^{N_s-1}\frac{|S_i|}{|S_i|_{\max}+\epsilon}\right)^{\alpha} \quad (29)$$

to reduce the transferred residual error. Instead of the transfer operators defined by Eq. (20) now

$$\begin{aligned}\bar{I}_{k\mapsto k+1}\mathbf{R}^k &= \sum_{l=1}^{4}\mathbf{R}^k_l\max\left[0,\min\left(1-\kappa^k_l,\,1-B^k\gamma^k_l\right)\right]\\ \bar{I}_{k\mapsto k+1}\mathbf{V}^k &= \sum_{l=1}^{4}\mathbf{V}^k_l\max\left[0,\min\left(1-\kappa^k_l,\,1-B^k\gamma^k_l\right)\right]\end{aligned} \quad (30)$$

is used. Such a local damping was preferred to the global one presented in Ref. [24]. Combustion is often limited to small regions, thus allowing the full multigrid scheme to work outside combustion zones. $|S_i|_{\max}$ is the maximum absolute production rate of species i within the flowfield, B^k is a grid level-dependent constant, and ϵ again is a small number to avoid division by zero. It is found to be advantageous that all individual production rates contribute to this sensor which is limited to $0\le\gamma\le 1$. An important condition for the sensor to work is its smooth distribution. An exponent α of 0.25 worked satisfactory for all test cases described later. A further possibility to improve convergence of the multigrid scheme is to perform the above described damping for the species residual errors only. This results in a decoupling in time between continuity and species conservation equations. However, steady state solutions are unaffected by such a treatment.

4.2.1. Assessment of different approaches. All methods which keep parts or the total chemical source vector or source Jacobian constant suffer from the extremely strong coupling between chemistry and fluid motion. Changes within species concentrations or temperature not being reflected within the parts kept constant are the major drawbacks of approaches 1 to 3. These methods worked for all investigated test cases employing up to

three grid levels and a time step reduction on the third grid. A fourth grid level always aggravated the results. Therefore, we prefer the simple local damping of approach 4. A disadvantage of this method is the strong case dependence of the choice of parameters B^k and α to limit the degree of damping. The reductions in CPU time achieved by using a fourth grid level are small but there still is an improvement.

While strong reductions in CPU time are obtained for attached flames, results for detached flames are still unsatisfactory. If the point of ignition is determined by chemical kinetics, differences between the grid levels destroy convergence. With approach 3 we hoped to localize ignition on coarse grids with reaction rates determined from the finest grid. However, no satisfactory results could be achieved with this method for detached flames.

5. RESULTS AND DISCUSSION

Numerical tests are performed to evaluate efficiency and robustness of the presented multigrid method for turbulent supersonic flows. All computations are initialized by fixing the inflow properties in the interior of the domain. The first set simulates nonreactive flows to demonstrate the ability of the multigrid technique to treat shock waves as well as source terms due to turbulent production. Next, three simulations are presented which include source terms due to both turbulence and chemistry. These test cases cover premixed and diffusion-dominated hydrogen combustion. All converged solutions of single and multigrid calculations are identical. The employed 20-step reaction mechanism [25] results in a numerical stiff system of governing equations. The maximum cell species Damköhler numbers $Da_i = (l_{\text{ref}} S_i)/(\rho\sqrt{u^2 + v^2})$ are 18.9, 1.1, and 24.1 for the first, second, and third test case. The reference length l_{ref} was chosen to be 1 cm. The maximum ratio of maximum to minimum species Damköhler numbers within any volume is up to 10^9. For comparison the last two test cases also show convergence rates of nonreactive calculations.

5.1. *Ramped Ducts with and without Separation*

Three planar ramped duct test cases without combustion are calculated and compared with experimental data of Settles *et al.* [39, 40]. In accordance with the experiment the angles of the compression corners are 8°, 16°, and 20°. The inflow Mach number is 2.85, and inflow static temperature and pressure are 100 K and 0.229 bar, respectively. All simulations start 6.2 cm upstream of the ramp ($x = 0$ is located at the corner) using calculated, fully developed turbulent inflow profiles matching the experimentally measured boundary layer thickness of $\delta = 2.1$ cm. The computational grid contains 152×80 volumes and is strongly refined at the wall and in the separation zone near the corner. All values of the normalized distance to the wall, y^+, are smaller than 0.6 at stationary condition. Such a level of refinement is required by most low-Reynolds-number turbulence models for an accurate resolution of the viscous sublayer. The resulting cell aspect ratios on the surface are as high as 4500. While the flow over the 8° ramp is still attached, a very small separation zone occurs for the 16° ramp, and the flow is separated over a region of about 18 mm for the 20° ramp. With increasing separation zone, turbulent production and dissipation terms increasingly dominate the turbulence conservation equations. Figure 1 shows a comparison between experimental and calculated normalized wall static pressure profiles. With the exception of the 20° ramp, where the increase in pressure in front of the separation zone is located too far downstream, the results compare quite well. Skin friction distributions are illustrated in

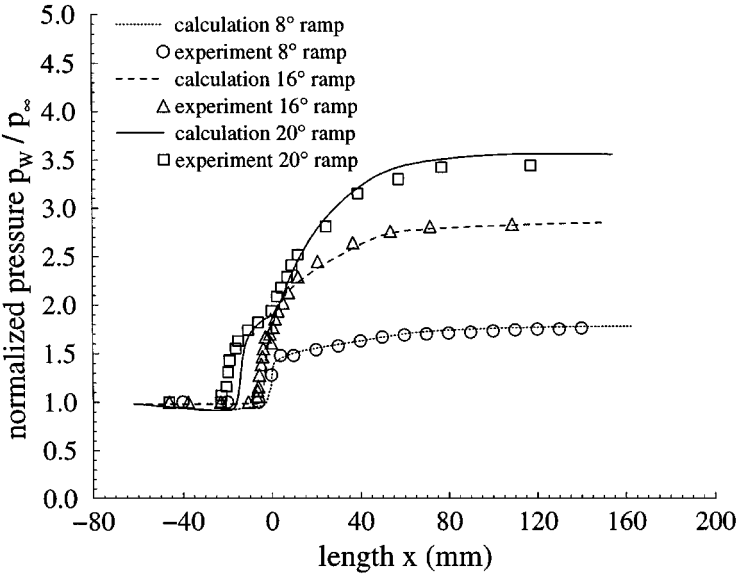

FIG. 1. Normalized surface static pressure distributions for ramped duct test cases.

Fig. 2. The results indicate that the predicted increase in skin friction after separation is too steep in comparison to the experiment. The good overall agreement between experiment and simulation makes the q-ω model interesting due to its favorable properties in conjunction with multigrid methods.

Convergence behavior of the calculations is displayed in Figs. 3 and 4. Plotted are the averaged absolute residuals of the continuity and q (turbulence) conservation equations versus the number of multigrid cycles. A four-level V-cycle multigrid method with two coarse grid iterations is employed, commencing on the finest grid. It may be seen that fluid and turbulence residuals converge at nearly the same rate. This is valid for all investigated test cases and is an advantage if all equations are treated with the multigrid technique. According to Eq. (20) the transferred residual errors are damped in the vicinity of shock waves. While the damping factors κ^k are zero in the smooth parts of the flowfield, they may approach one near shock waves. For the 20° ramp the maximum value κ^k at stationary condition out of all volumes is 0.27, 0.63, and 0.89 for the transfer from first to second, second to third, and third to fourth grid level, respectively. An unfavorable property of the LU-SGS scheme may also be observed from Fig. 3. With the occurrence of a large separated region for the 20° ramp and subsequently a large pocket of subsonic flow, the convergence rate of the algorithm degrades. This is due to an increased amount of upwind influence [41]. If the multigrid method is employed, convergence histories also differ due to flow separation. However, machine accuracy is obtained after the same number of multigrid cycles. Convergence histories of the density residuals in terms of work units are plotted in Fig. 5. One work unit is defined as the computational time necessary for one fine grid iteration. Because all computations are performed on vector computers (Cray C94 and NEC-SX4) using a fully vectorized code, reductions achieved in CPU time are smaller than the theoretically possible values. This is due to shorter vector lengths on coarse grids reducing the performance of the code. However, the convergence improvement relative to the single grid iteration is at least threefold.

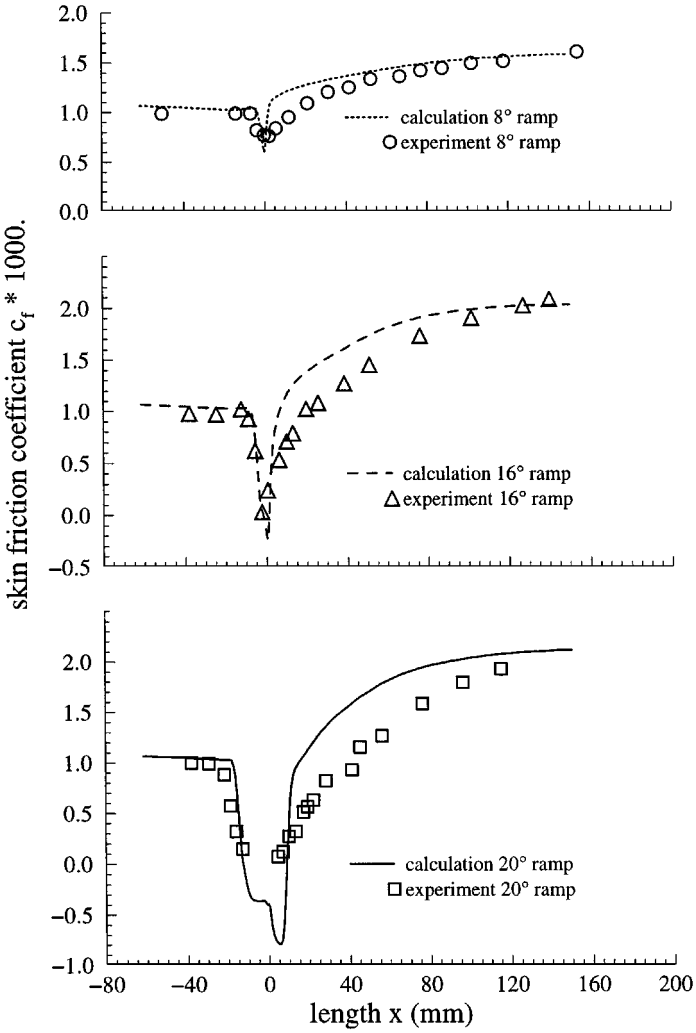

FIG. 2. Surface skin friction distributions for ramped duct test cases ($c_f = 2\tau_W/(\rho_\infty u_\infty^2)$).

5.2. *Oblique Detonation Wave*

The first test case including finite-rate chemistry is a supersonic Mach 5 flow over a wedge with 26.5° half angle (see Fig. 6). The inflow conditions are a static pressure and temperature of 0.324 bar and 450 K, respectively. Hydrogen and air are premixed at an equivalence ratio of 0.6. Due to these inflow conditions a stationary stable detonation wave is obtained. An Euler solution for the same problem may be found in Ref. [42]. A 1-block grid containing 120×80 volumes is used for this calculation. The minimum normal spacing for the grid at solid walls is 1.7×10^{-6} m, fine enough to ensure y^+ values smaller than 0.7 even at the tip of the wedge. The refinement near the solid wall results in cell aspect ratios of up to 2100. For detonation waves there is a direct coupling between the increase in pressure due to the shock wave and the increase in pressure due to heat release from combustion. Downstream of the detonation wave, combustion is nearly completed. According to our experience the detonation wave angle strongly depends on the finite-rate chemistry model used and is determined by the amount and speed of heat release due to combustion. Figure 7 shows

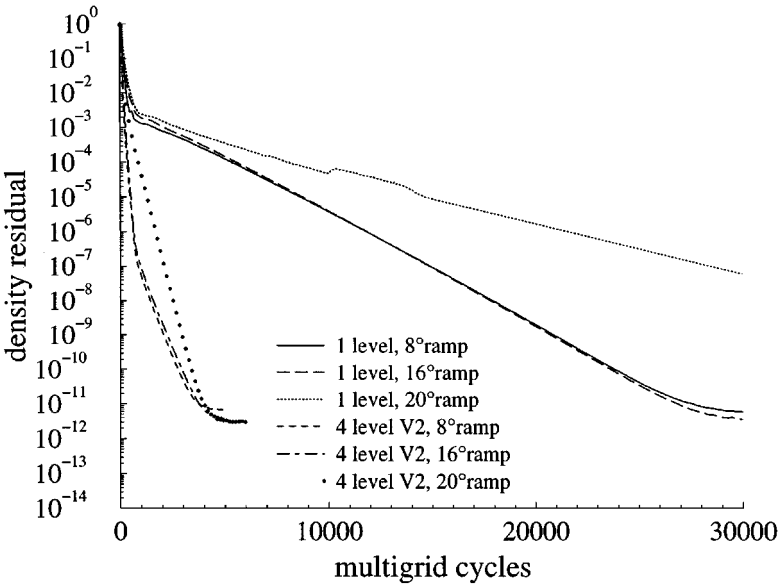

FIG. 3. Convergence histories of the density residuals for nonreactive ramped duct test cases versus the number of multigrid cycles.

pressure profiles along the cut line $y = 6.6$ cm for $x \leq 10$ cm and $y = 0.334x + 3.26$ cm for $x > 10$ cm. The differences between the present calculation and those of Ref. [42] mainly result from different reaction schemes and subsequent different detonation wave angles. By use of a simpler 8-step reaction scheme instead of the 20-step reaction scheme the same angle and shock location was obtained as in Ref. [42], where a 9-step reaction scheme is employed. Mass fraction profiles of H_2, H_2O, O_2 and OH are plotted in Fig. 8.

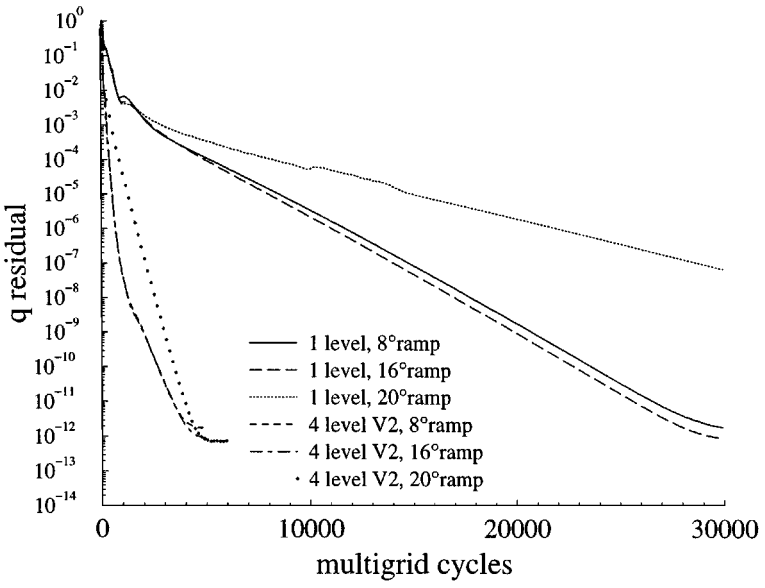

FIG. 4. Convergence histories of the q residuals for nonreactive ramped duct test cases versus the number of multigrid cycles.

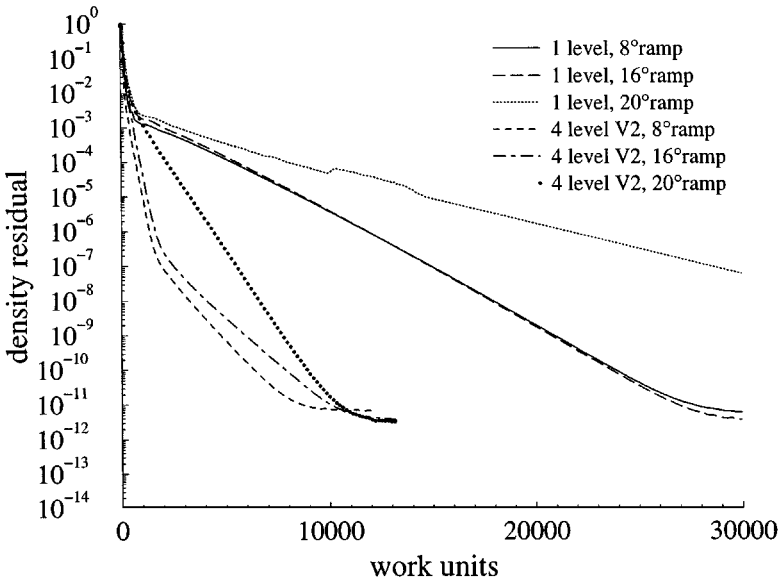

FIG. 5. Convergence histories of the density residuals for nonreactive ramped duct test cases versus the number of work units.

From a numerical point of view an attached detonation wave is less critical for the use of multigrid methods than diffusion-dominated flows. In such cases combustion only takes place in a spatially very limited zone coupled with strong gradients in static pressure. This simplifies the calculation of sensors to locate main reaction zones. The chemically slow combustion downstream of the detonation wave did not cause any problem for the multigrid method. All four proposed approaches worked well for this test case using a nested four-level V-cycle multigrid algorithm. Moreover, the described standard residual error damping and time step reduction at shock waves (see Eqs. (20) and (23)) already enable convergence. This demonstrates the possibility to achieve convergence of a multigrid method by blending off the transferred residual error in critical regions. On the other hand every reduction of coarse grid information degrades the achievable acceleration rates, making optimum damping parameters desirable. If the damping factors $1 - \kappa^k$ (see Eq. (20)) are multiplied with the cell volume, added, and normalized with the total flowfield area, the average damping

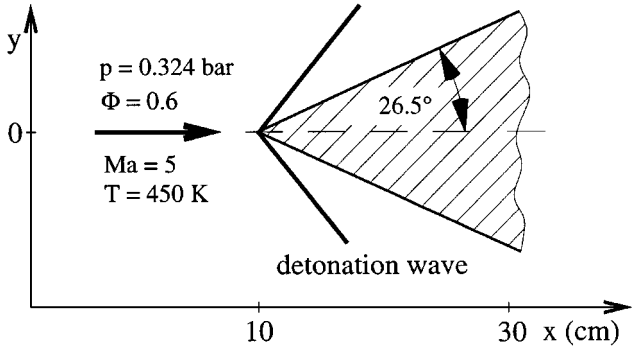

FIG. 6. Geometry and inflow conditions for detonation wave simulation.

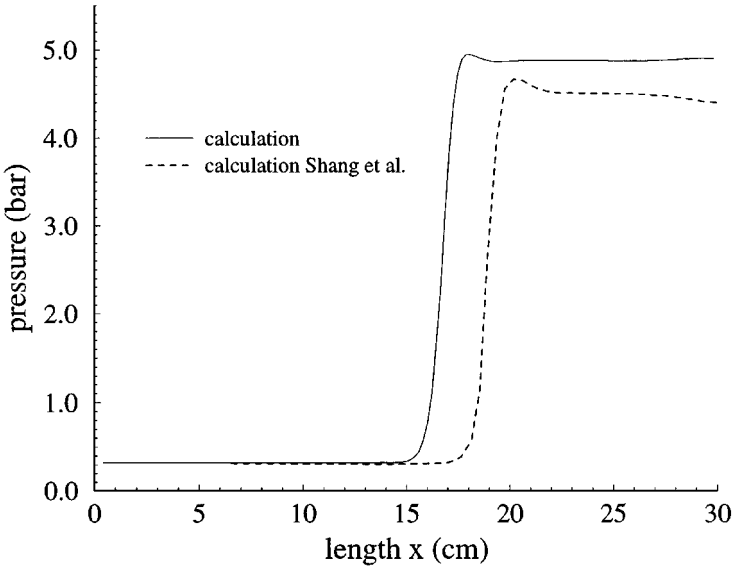

FIG. 7. Pressure profiles along cut line for detonation wave simulation.

factor during restriction from grid level one to two is 0.82, that from level two to three is 0.87, and that from level three to four is 0.75. Similar values are obtained for the average reduction of coarse grid time steps. However, a locally strong damping near the detonation wave limits the information passed, thus retarding convergence. Convergence histories of the normalized absolute density residual versus the number of work units are illustrated in Fig. 9. One four-level V-cycle is roughly 2.39 times as expensive as one fine grid iteration. Convergence improvement relative to the single grid solution is more than a factor of 2 in CPU time.

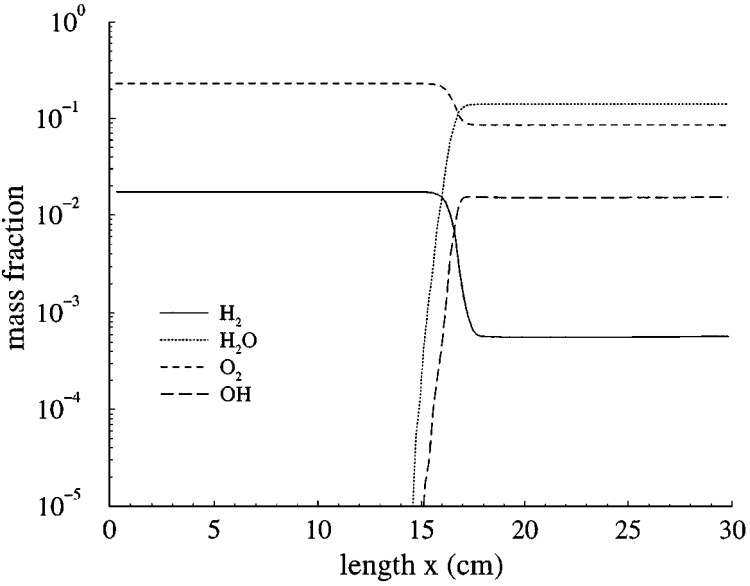

FIG. 8. Mass fraction profiles along cut line for detonation wave simulation.

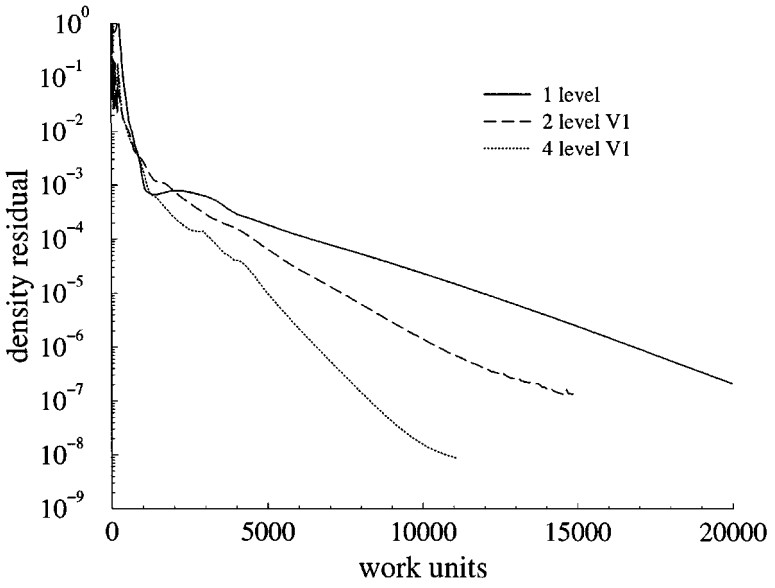

FIG. 9. Convergence histories of the density residuals for detonation wave calculations versus the number of work units.

5.3. *Plane Reactive Shear Flow*

More severe problems for multigrid techniques arise if diffusion-dominated flames are treated. The following model problem [43] corresponds to a supersonic shear flow over a splitter plate with a 4° angle (see Fig. 10). Precalculated, fully turbulent inlet profiles with $\delta = 0.5$ cm boundary layer thickness are used for both streams. Pertinent inflow conditions of the upper air and the lower hydrogen/nitrogen stream are summarized in Table I. The flow is characterized by its high inflow temperatures which cause ignition directly at the tip of the splitter plate. The simulation starts 4 cm upstream of the tip, employing a two block grid with 128×64 volumes for each block. Due to the requirements of turbulence model

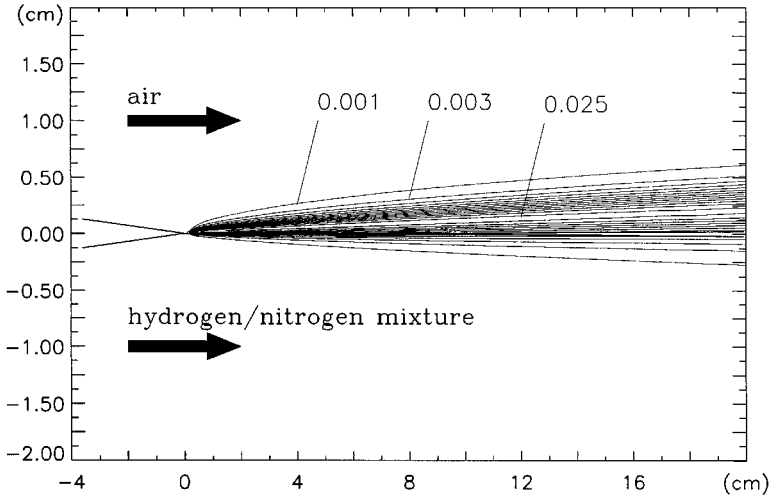

FIG. 10. Calculated contours of OH mass fractions for plane reactive shear flow.

TABLE I
Inflow Conditions for the Upper Air and Lower Hydrogen/Nitrogen Stream

	Upper air stream	Lower H_2/N_2 stream
p (bar)	1	1
u (m/s)	1800	2697
T (K)	2000	2000
Y_{H_2}	0	0.1
Y_{N_2}	0.7664	0.9
Y_{O_2}	0.2336	0

and flow characteristic the grid is highly clustered near solid walls, at the tip of the splitter plate, and in the combustion zone, resulting in cell aspect ratios of up to 2200. All y^+ values of near wall cell centers are smaller than 0.2. Figure 10 shows calculated OH mass fraction contours indicating the main combustion zone.

Figures 11 and 12 illustrate convergence histories of the density residuals versus the number of multigrid cycles and work units, respectively. One four-level V-cycle is roughly 2.34 times as expensive as one fine grid iteration. All calculations up to the second grid level are performed without modifications due to chemistry. As already mentioned, approaches 1 to 3 suffer from the parts kept constant in source term and source Jacobian. The use of a third grid level already destroyed or aggravated convergence. However, a further improvement in comparison to the two-level multigrid is achieved by a global time step reduction on the third grid level. No improvement was obtained employing a fourth grid level. For this test case approaches 1 to 3 achieved quite similar results. The disadvantage of the first three approaches is a strong sensitivity to flow conditions, such as grid spacing and resolution of

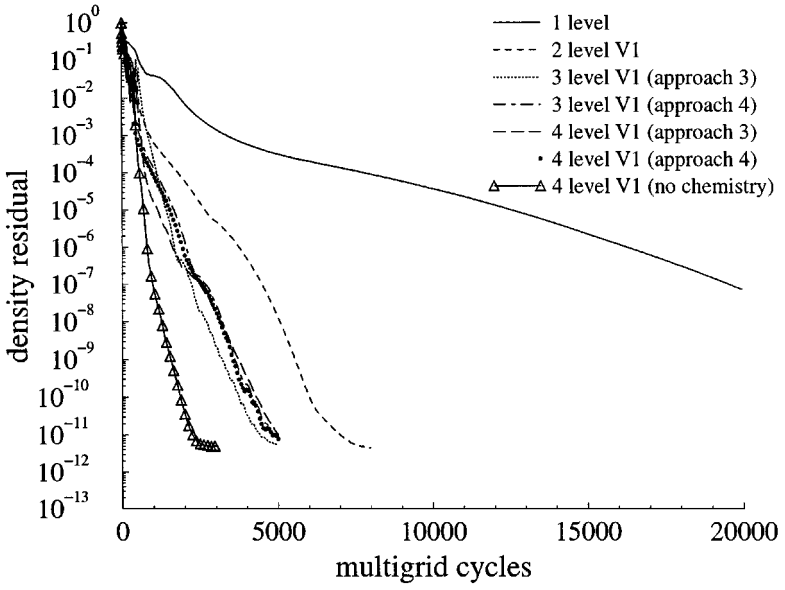

FIG. 11. Convergence histories of the density residuals for planar nonreactive and reactive shear flows versus the number of multigrid cycles.

the combustion zone. Even if the best results for this test case could be achieved by approach 3 and three grid levels, approach 4 is recommended because of its higher stability. As for the first three approaches, a four-level multigrid did not improve the convergence using approach 4 but at least achieved about the same acceleration as the three level multigrid method. The greatest problem is the optimum choice of damping parameters because these input values define the degree of convergence acceleration. Nevertheless, improvement in terms of CPU time in comparison to the single grid iteration is slightly better than threefold.

5.4. *Axisymmetric Shear Flow*

The final test case considered corresponds to an experiment of Evans *et al.* [44]. Figure 13 illustrates the axisymmetric hydrogen injection into a preheated vitiated air stream. A three-block grid is chosen to resolve the lip thickness at the end of the injector. The grid contains 136×72, 112×48, and 136×48 volumes to simulate the upper half of the symmetric problem. The calculation starts at $x = -0.33$ cm, thus simulating the inner and outer boundary layers at the tube surfaces (see Fig. 15). Precalculated, fully turbulent boundary layer profiles are specified as inflow conditions. The computational grid is highly clustered near solid walls as well as in the recirculation zone at the end of the tube. The minimum radial spacing is 1×10^{-6} m, fine enough to ensure y^+ values smaller than 0.8 for the converged solution. The highest cell aspect ratio is about 500. The inflow conditions of the pure hydrogen and the vitiated air are summarized in Table II. Figures 14 and 15 show calculated temperature and pressure contours to illustrate some overall features of the flowfield. Expansion fans are formed at the outer and inner rims at the end of the tube, followed by shock waves (see Fig. 15). A strongly refined grid arrangement is necessary to resolve these features which may be important for ignition. Species profiles have been measured at four different streamwise locations. One of these profiles is plotted in Fig. 16.

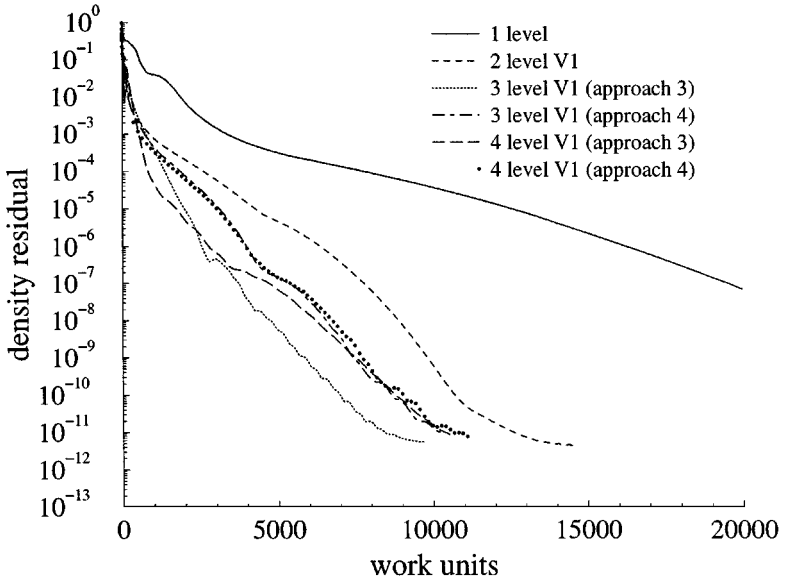

FIG. 12. Convergence histories of the density residuals for planar reactive shear flows versus the number of work units.

TABLE II
Inflow Conditions for Axisymmetric Combustion Experiment of Evans *et al.* [44]

	Hydrogen jet	Vitiated air stream
p (bar)	1	1
u (m/s)	2432	1510
T (K)	251	1495
Ma	2	1.9
Y_{H_2}	1	0
Y_{H_2O}	0	0.281
Y_{N_2}	0	0.478
Y_{O_2}	0	0.241

The best convergence histories are obtained by damping the transferred residuals of the multigrid method in regions of intense chemistry (approach 4). This method is only applied for restriction at grid levels higher than two. For the same test case Edwards [24] obtained best results for a seven-species calculation with two grid levels and for a nine-species calculation with three grid levels. The proposed application of local damping of the restricted residual error still achieves improved convergence rates by the application of a four-level V-cycle multigrid algorithm. Additionally, we found it feasible to reduce the damping factor γ (see Eq. (29)) as the solution approaches the stationary condition. When the residual has dropped more than one order in magnitude, γ is reduced in a logarithmic way until, after a drop of five orders in magnitude, γ is set to zero. At this point the full four-level multigrid is working. Note, however, that there is still a reduction in transferred residual error and time step ($n = 1$ in Eq. (23)) in the vicinity of shock waves. The benefits of the multigrid algorithm are demonstrated in Figs. 17 and 18. Given are the convergence histories for density and q residuals versus the number of multigrid cycles and work units, respectively. It appears that one multigrid cycle requires 2.26 times the time of

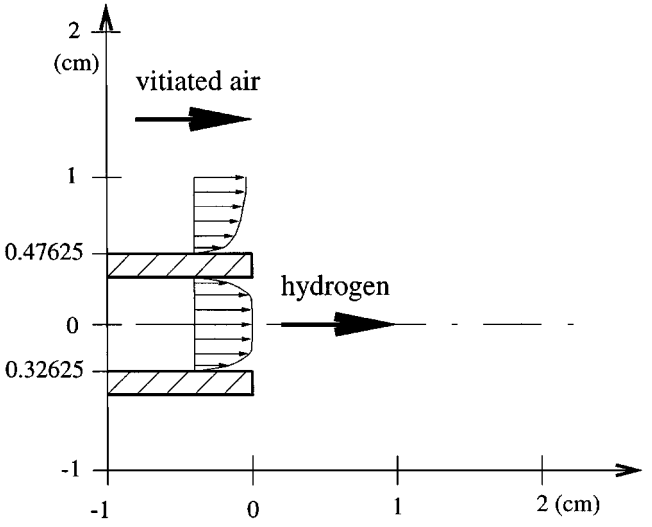

FIG. 13. Geometry (cm) for the Evans *et al.* [44] axisymmetric combustion experiment.

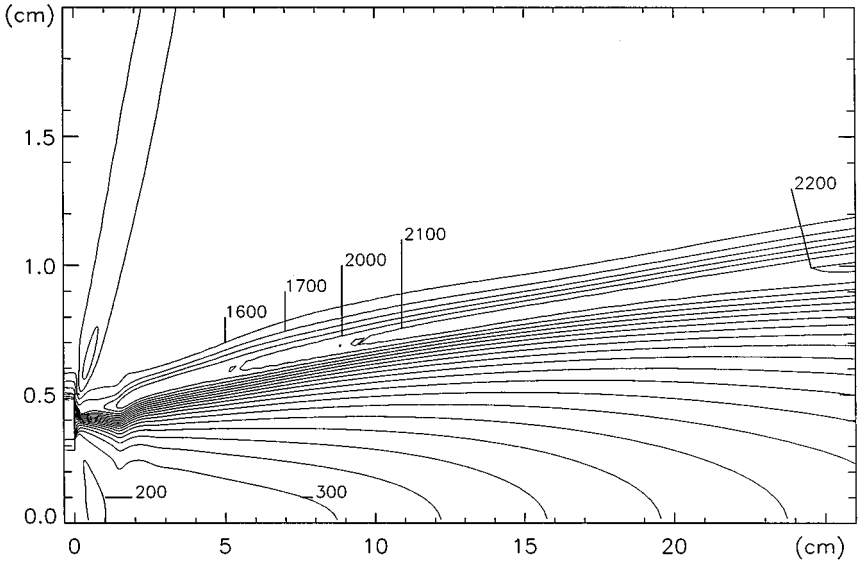

FIG. 14. Calculated temperature contours (K) for the Evans *et al.* [44] experiment.

one fine grid iteration. As in the previous cases this factor is grid size dependent and much higher than the theoretically possible value due to short vector lengths on coarse grids. Thus, still better convergence rates may be expected if scalar computers are employed. The four-level nested multigrid algorithm converges about three times faster than the one-grid solution.

6. CONCLUSIONS

An implicit multigrid method has been successfully applied to supersonic reactive flows using a low-Reynolds-number q-ω turbulence model as well as 20-step finite-rate chemistry. All conservation equations are treated with the multigrid technique. This algorithm is robust in handling very small grid spacings and high aspect ratio grids, necessary for

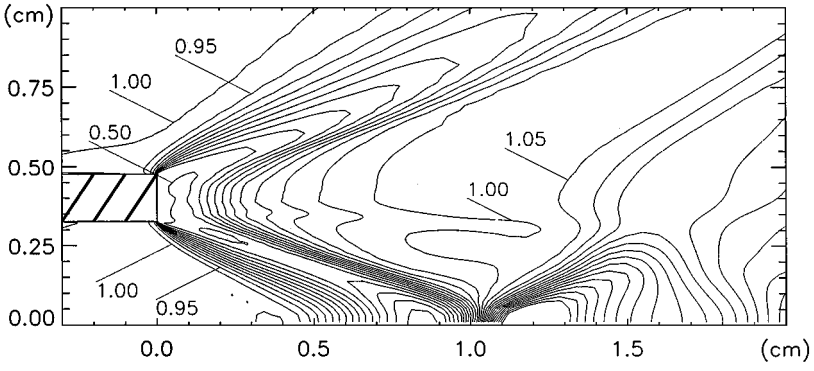

FIG. 15. Calculated pressure contours (bar) near the injector for the Evans *et al.* [44] experiment.

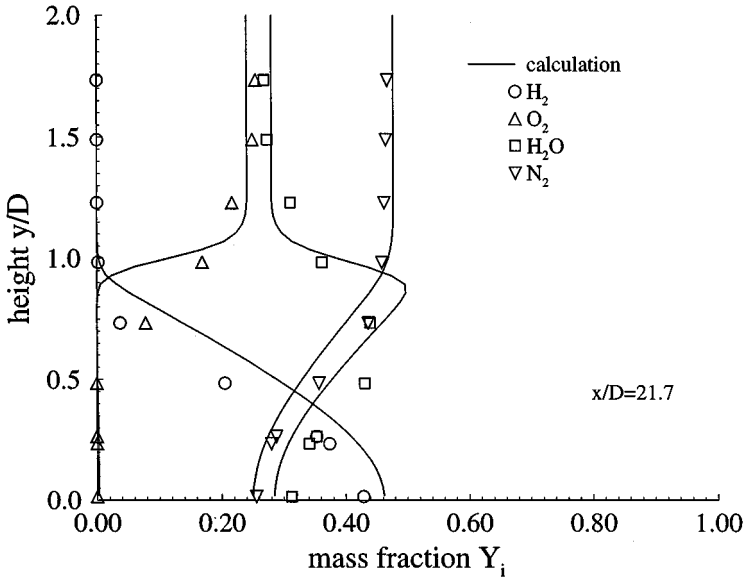

FIG. 16. Profiles of H_2, O_2, H_2O, and N_2 molar fractions at $x/D = 21.7$ for the Evans *et al.* [44] experiment (diameter $D = 0.9525$ cm).

high-Reynolds-number flows. Modifications to standard multigrid methods are used to avoid unphysical upwind influences near shock waves. Turbulent source terms are treated by freezing strongly nonlinear parts on coarse grids. Several approaches are investigated to treat the chemical source terms in order to extend multigrid methods to reacting flows. A simple local damping of the restricted residual error together with a time step reduction

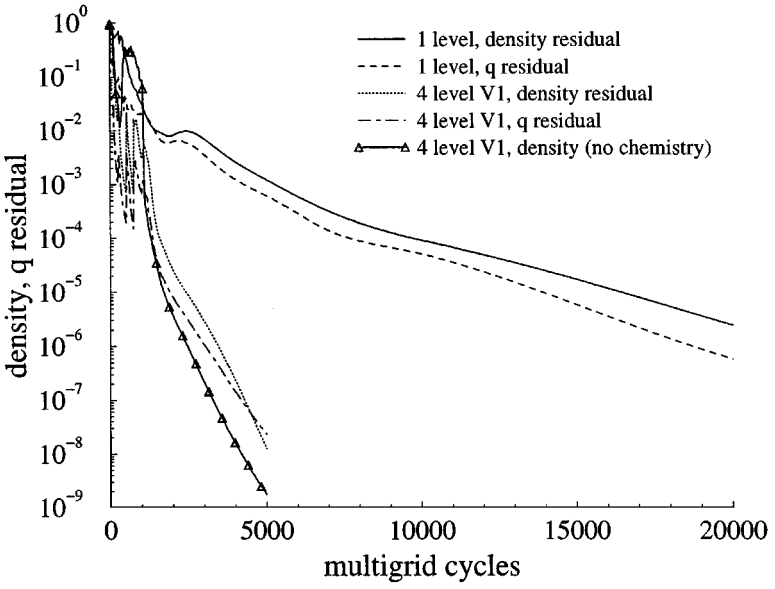

FIG. 17. Convergence histories of the density and q residuals for the Evans *et al.* [44] experiment versus the number of multigrid cycles.

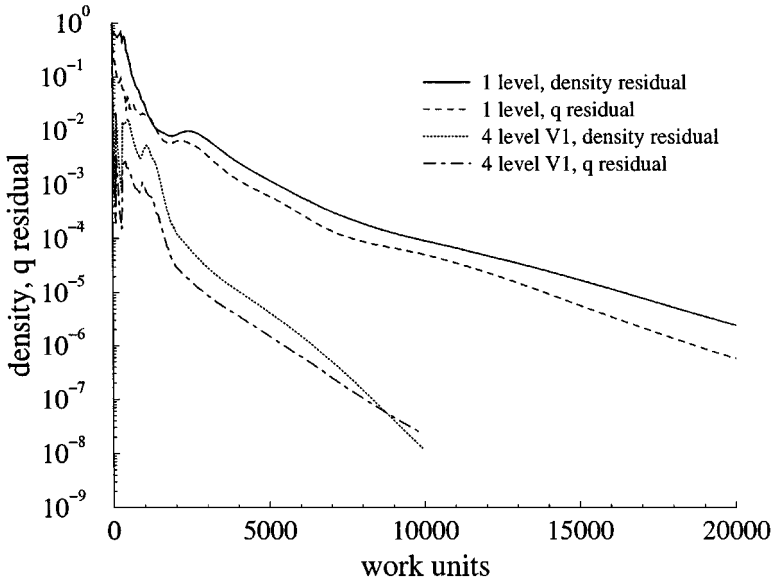

FIG. 18. Convergence histories of the density and q residuals for the Evans *et al.* [44] experiment versus the number of work units.

in regions of high chemical intensity achieved best results for all investigated hydrogen flames. While the treatment of turbulent source terms is very robust from a numerical point of view, the chemistry still remains quite sensitive to the choice of local damping parameters. In addition, there are severe problems in simulating detached flames. The calculation of several test cases has demonstrated the ability of the proposed nested multigrid method to speed up convergence to a steady state by a factor of three in CPU time for attached flames and low-Reynolds-number turbulence closure.

ACKNOWLEDGMENTS

We thank the Deutsche Forschungsgemeinschaft (DFG) for the financial support of this work within the SFB 259 at the University of Stuttgart. Parts of this work were performed during the first author's stay at North Carolina State University. This author thanks Professor H. A. Hassan for the possibility to work with him and his group.

REFERENCES

1. W. Hackbusch, *Computational Mathematics (4)* (Springer-Verlag, Berlin/Heidelberg/New York, 1985).
2. A. Brandt, Multi-level adaptive solutions to boundary-value problems, *Math. Comp.* **31**, 333 (1977).
3. S. W. McCormick, Ed., *Frontiers in Applied Mathematics Series* (SIAM, Philadelphia, 1987).
4. A. Jameson and S. Yoon, Lower–upper implicit schemes with multiple grids for the Euler equations, *AIAA J.* **25**, 929 (1987).
5. L. Martinelli, A. Jameson, and F. Grasso, *A Multigrid Method for the Navier–Stokes Equations*, AIAA Paper 86-0208 (unpublished).
6. R. C. Swanson, E. Turkel, and J. A. White, *An Effective Multigrid Method for High-Speed Flows*, NASA ICASE Report 91-56, 1991 (unpublished).
7. E. Turkel, R. C. Swanson, V. N. Vatsa, and J. A. White, *Multigrid for Hypersonic Viscous Two- and Three-Dimensional Flow*, NASA ICASE Report 91-57, 1991 (unpublished).

8. V. N. Vatsa, E. Turkel, and J. S. Abolhassani, Extension of multigrid methodology to supersonic/hypersonic 3-D viscous flows, *Int. J. Numer. Methods Fluids* **17**, 825 (1993).
9. P. W. Hemker and B. Koren, *Defect Correction and Nonlinear Multigrid for the Euler Equations*, Lect. Series 1988-05 (von Karman Institute for Fluid Dynamics, 1988).
10. J. R. Edwards, Upwind relaxation multigrid method for computing three-dimensional, viscous internal flows, *J. Prop. Power* **12**, 146 (1996).
11. M. P. Leclercq and B. Stoufflet, Characteristic multigrid method application to solve the Euler equations with unstructured and unnested grids, *J. Comput. Phys* **104**, 329 (1993).
12. B. Koren and P. W. Hemker, Damped, direction-dependent multigrid for hypersonic flow computations, *Appl. Numer. Math.* **7**, 309 (1990).
13. R. Radespiel and R. C. Swanson, Progress with multigrid schemes for hypersonic flow problems, *J. Comput. Phys.* **116**, 103 (1995).
14. P. Gerlinger and D. Brüggemann, Multigrid convergence acceleration for turbulent supersonic flows, *Int. J. Numer. Methods Fluids* **24**, 1019 (1997).
15. P. Gerlinger and D. Brüggemann, An implicit multigrid scheme for the compressible Navier–Stokes equations with low-Reynolds-number turbulence closure, *ASME J. Fluids Eng.* **120**, 257 (1998).
16. F. Liu and X. Zheng, A strongly coupled time-marching method for solving the Navier–Stokes and k-ω turbulence model equations with multigrid, *J. Comput. Phys* **128**, 289 (1996).
17. J. F. Slomski, J. D. Anderson, and J. J. Gorski, *Effectiveness of Multigrid in Accelerating Convergence of Multidimensional Flows in Chemical Nonequilibrium*, AIAA Paper 90-1575 (unpublished).
18. R. Radespiel, J. M. A. Longo, S. Brück, and D. Schwamborn, *Efficient Numerical Simulation of Complex 3D Flows with Large Contrast*, AGARD-CP-578 33-1 (1996).
19. C. Liao, Z. Liu, X. Zheng, and C. Liu, *NO_x Prediction in 3-D Turbulent Diffusion Flames by Using Implicit Multigrid Methods*, AIAA Paper 95-3166 (unpublished).
20. C. Liao, Z. Liu, and C. Liu, *Implicit Multigrid Method for Modeling 3-D Turbulent Diffusion Flames with Detailed Chemistry*, AIAA Paper 95-0801 (unpublished).
21. X. Zheng, C. Liao, Z. Liu, and C. Liu, Mass-fluxed-based implicit multigrid method for modeling multi-dimensional combustion, *J. Prop. Power* **13**, 97 (1997).
22. S. G. Sheffer, A. Jameson, and L. Martinelli, *A Multigrid Method for High Speed Reactive Flows*, AIAA Paper 97-2106 (unpublished).
23. J. R. Edwards, An implicit multigrid algorithm for computing hypersonic, chemically reacting viscous flows, *J. Comput. Phys.* **123**, 84 (1996).
24. J. R. Edwards, *Advanced Implicit Algorithms for Finite Rate Hydrogen–Air Combustion Calculations*, AIAA Paper 96-3129 (unpublished).
25. C. J. Jachimowski, *An Analytical Study of the Hydrogen–Air Reaction Mechanism with Application to Scramjet Combustion*, NASA TP 2791, 1988 (unpublished).
26. C. R. Wilke, A viscosity equation for gas mixtures, *J. Chem. Phys.* **18**, 517 (1950).
27. R. B. Bird, W. E. Steward, and E. N. Lightfood, *Transport Phenomena* (Wiley, New York, 1960).
28. T. J. Coakley, *Turbulence Modeling Methods for the Compressible Navier–Stokes Equations*, AIAA Paper 83-1693 (unpublished).
29. T. J. Coakley and P. G. Huang, *Turbulence Modeling for High Speed Flows*, AIAA Paper 92-0436 (unpublished).
30. P. Gerlinger, J. Algermissen, and D. Brüggemann, Numerical simulation of mixing for turbulent slot injection, *AIAA J.* **34**, 73 (1996).
31. J. S. Shuen, Upwind differencing and LU factorization for chemical non-equilibrium Navier–Stokes equations. *J. Comput. Phys.* **99**, 233 (1992).
32. A. Jameson and S. Yoon, Multigrid solution of the Euler equations using implicit schemes, *AIAA J.* **24**, 1737 (1986).
33. S. Eberhardt and S. Imlay, *A Diagonal Implicit Scheme for Computing Flows with Finite-Rate Chemistry*, AIAA Paper 90-1577 (unpublished).

34. R. C. Swanson and E. Turkel, On central difference and upwind schemes, *J. Comput. Phys.* **101**, 292 (1992).
35. P. Gerlinger, J. Algermissen, and D. Brüggemann, Matrix dissipation for central difference schemes with combustion, *AIAA J.* **33**, 1865 (1995).
36. A. Brandt, *Multi-Level Adaptive Solutions in Fluid Dynamics*, INKA-Conf.-79, 351-010, 79-1455 (1979).
37. A. Jameson, W. Schmidt, and E. Turkel, *Numerical Solution of the Euler Equations by Finite Volume Methods Using Runge–Kutta Time Stepping Schemes*, AIAA Paper 81-1259 (unpublished).
38. P. Gerlinger and D. Brüggemann, A robust implicit multigrid method for the simulation of turbulent supersonic mixing, submitted for publication.
39. G. S. Settles, T. J. Fitzpatrick, and S. Bogdonoff, Detailed study of attached and separated compression corner flowfields in high Reynolds number supersonic flow, *AIAA J.* **17**, 579 (1979).
40. E. Roshotko, Ed., *A Survey of Measurements and Measuring Techniques in Rapidly Distorted Compressible Turbulent Boundary Layers*, AGARD-AG-315 12A-1 (1989).
41. J. Edwards, *Nonlinear Relaxation Algorithms for the Compressible Navier–Stokes Equations in Two and Three Dimensions*, Ph.D. thesis, North Carolina State University, 1992 (unpublished).
42. H. M. Shang, Y. S. Chen, Z. J. Chen, C. P. Chen, and T. S. Wang, *Numerical Studies of Finite-Rate Reacting Flows with a Pressure Based Method*, AIAA Paper 94-3048 (unpublished).
43. J. R. Narayan and S. S. Girimaji, *Turbulent Reacting Flow Computations Including Turbulence Chemistry Interactions*, AIAA Paper 92-0342 (unpublished).
44. J. S. Evans, C. J. Schexnayder, and H. J. Beach, *Application of a Two-Dimensional Parabolic Computer Program to Prediction of Turbulent Reacting Flows*, NASA TP 1169, 1978 (unpublished).